Available online at www.sciencedirect.com
ScienceDirect
Polymer 48 (2007) 2144–2154
polymer
www.elsevier.com/locate/polymer

Effects of clay on phase morphology and mechanical properties in polyamide 6/EPDM-*g*-MA/organoclay ternary nanocomposites

Ke Wang, Cong Wang, Jiang Li, Juanxia Su, Qin Zhang, Rongni Du, Qiang Fu*

Department of Polymer Science and Materials, State Key Laboratory of Polymer Materials Engineering, Sichuan University, Chengdu 610065, People's Republic of China

Received 1 November 2006; received in revised form 28 December 2006; accepted 27 January 2007
Available online 7 February 2007

Abstract

In this study, both organoclay and EPDM-*g*-MA rubber were used to simultaneously improve the toughness and stiffness of polyamide 6 (PA6). We first prepared PA6/EPDM-*g*-MA/organoclay ternary nanocomposites using melt blending. Then the composites were subjected to traditional injection molding and so-called dynamic packing injection molding. The dispersion of clay, phase morphology, crystallinity and orientation of PA6 as well the mechanical properties were characterized by WAXD, SEM, DSC, 2D-WAXS and mechanical testing, respectively. The effects of clay on phase morphology and mechanical properties of PA6/EPDM-*g*-MA blends could be summarized as follows: (1) weakening interphase adhesion between PA6 and EPDM-*g*-MA rubber particles, resulted in increasing of rubber particle size, as the clay and rubber contents are low; (2) preventing coalescence of rubber domains, arisen in decreasing of rubber particle size, as the clay and rubber contents are high; (3) the blocking effect on the overlap of stress volume around rubber particles caused broadening of the brittle–ductile transition region and decrease of toughness, and (4) the effective stress transfer leading a better reinforcement when the interparticle distance is smaller than the critical value.

Keywords: Organoclay; Polyamide 6; Blocking effect

1. Introduction

In recent years, many inexpensive types of clay such as montmorillonite (MMT) have been extensively used for preparation of polymer nanocomposites [1–5]. After treated with cationic surfactants, hydrophilic silicate particles can be dispersed into individual layers in the hydrophobic polymers. Due to some advanced properties such as enhanced tensile/flexural strength, thermal and barrier properties, lots of studies on nanocomposites with a single polymer matrix have been carried out [6–10]. However, the incorporation of clay usually results in a deterioration of the strain-related end properties such as notched impact strength, which is already low in some single polymers, for example, polypropylene and polyamide 6. In order to achieve satisfied balanced properties, ternary nanocomposites have attracted great attention in both academic and industry [11–18].

Researches on ternary nanocomposites are mainly focused on three directions. The first one is to investigate the role of organoclay in phase behavior of immiscible polymer blends and it is still controversy concerning its mechanism [11,12]. The explanations of reduction of domain size with the addition of organoclays include the combination of partial compatibilization by excessive surfactant in organoclays and increased viscosity [11], the emulsification effect of organoclay [12], the fact that two immiscible polymer chains can exist together between the intercalated clay platelets and thus these two chains play the role of a block copolymer [13], and the coalescence preventing effect of exfoliated platelets on the dispersed domains [14]. The second direction is to investigate the effect of improved compatibilization achieved by the addition of

* Corresponding author. Tel./fax: +86 28 85405402.
E-mail address: qiangfu@scu.edu.cn (Q. Fu).

0032-3861/$ - see front matter © 2007 Elsevier Ltd. All rights reserved.
doi:10.1016/j.polymer.2007.01.070

a third component (i.e. compatibilizer) or by in situ chemical reaction between blended components on the properties of nanocomposites [15]. The compatibilized nanocomposites have shown a more homogeneous morphology and better clay dispersion than the uncompatibilized counterparts and thus resulting in a significant improvement in the strength and stiffness of composites. The third direction is to investigate the approaches of toughening in ternary nanocomposites and the corresponding toughening mechanism [16]. González et al. [17] studied compatibilization level effects on the critical interparticle distance (τ_c) and found that τ_c decreases with the content of maleic anhydride (MA) grafted rubber. In addition to add rubber grafted with maleic anhydride [16,17], blending sequence also affected the toughness through various microstructures [18].

Some drawbacks such as low distortion temperature (LDT) and brittleness of polyamide 6 (PA6) have limited its application, so lots of researches have been done on the improvement of these properties. Incorporating with rubber could achieve satisfied toughness but results in a decreased modulus and tensile strength. Whereas, compounding with organoclay could enhance the modulus and stiffness but decreases the toughness. In order to achieve balanced mechanical properties, in this work, both EPDM-*g*-MA rubber and organoclay have been used to prepare the PA6/EPDM-*g*-MA/clay ternary nanocomposites. Our focus is to study the effect of organoclay on toughening and reinforcing of PA6/EPDM-*g*-MA/organoclay ternary nanocomposites. Both traditional injection molding and an unique processing method, so-called dynamic packing injection molding (DPIM), in which the melt is first injected into the mold and then forced to move repeatedly in a chamber by two pistons that move reversibly with the same frequency as the solidification progressively occurs from the mold wall to the molding core part [19–21], were used to prepare the tested samples. The dispersion of clay, phase morphology, crystallization and orientation of PA6 and the mechanical properties were investigated and compared between these two processing methods.

2. Experimental

2.1. Material

Polyamide 6 (B3S) with a density of 1.13 g/cm^3 and a melt flow index (MFI at 230 °C and 2.16 kg loading) of 36 g/10 min was obtained commercially from BASF Company. Ethylene–propylene–diene copolymer grafted with maleic anhydride (EPDM-*g*-MA, CG700) was provided by Chen-Guang chemical institution; the grafted rate and the density were 0.92 wt% and 0.84 g/cm^3, respectively, with a melt flow index (MFI at 230 °C and 2.16 kg load) of 5 g/10 min. Sodium montmorillonite with a cation exchange capacity (CEC) of 68.8 mmol/100 g (RenShou, Sichuan, China) was organically modified through ion-exchange reaction with dioctadecyl dimethylammonium bromide and the detailed procedure could be found in our previous publication [22]. The modified MMT was denoted as organoclay throughout this paper.

2.2. Specimens preparation

To find the effect of blending sequence on mechanical properties of nanocomposites, four blending sequences were adopted: N1-(PA6 + EPDM-*g*-MA + organoclay), N2-(PA6 + EPDM-*g*-MA) + organoclay, N3-(PA6 + organoclay) + EPDM-*g*-MA, and N4-(EPDM-*g*-MA + organoclay) + PA6. For N1 all these three components were blended simultaneously while for N2, N3, and N4, the two components in bracket were blended first and then blended with the third component. The weight percentages of EPDM-*g*-MA and organoclay were 20 and 4, respectively. Moreover, the nanocomposites obtained from one step blending of PA6, EPDM-*g*-MA (5 wt%, 10 wt%, 15 wt%, 20 wt%, 25 wt%, 30 wt%, and 40 wt%), and organoclay (1 wt% and 4 wt%) were also prepared. All the blending experiments were carried out using a TSSJ-2S co-rotating twin-screw extruder. The barrel temperature and the screw speed were set at 190–220–230–230–220 °C and 120 rpm, respectively. The droplets got from extruder were molded both with DPIM and traditional injection molding for comparison under the same processing parameters. The schematic representation of DPIM is shown in Fig. 1. The obtained specimens are dumbbell shape. Some processing parameters in DPIM are listed in Table 1. The specimens obtained from DPIM and traditional injection moldings are called dynamic specimens and static specimens, respectively. Prior to extrusion and injection molding, all the materials were vacuum oven-dried for 24 h at 80 °C.

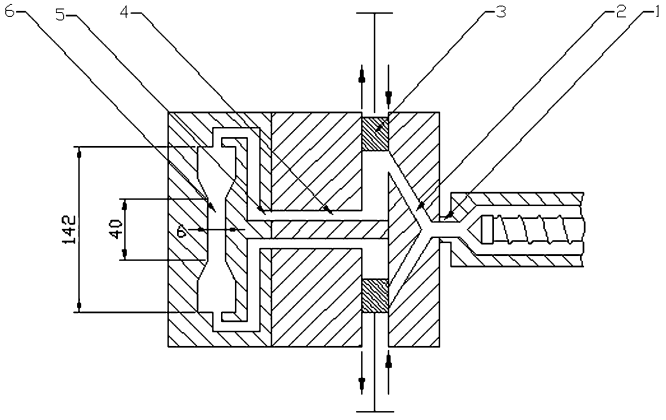

Fig. 1. The schematic representation of dynamic packing injection molding. (1) Nozzle, (2) sprue, (3) piston, (4) runner, (5) connector, and (6) specimen.

Table 1
Processing parameters in DPIM

Processing parameter	Parameter value
Injection pressure (MPa)	90
Packing pressure (MPa)	50
Melt temperature (°C)	240
Mold temperature (°C)	20
Dynamic packing pressure (MPa)	35
Dynamic packing frequency (Hz)	0.3

2.3. WAXD and 2D-WAXS measurements

The exfoliation level of montmorillonite was analyzed by a Siemens D500 diffractometer in reflection mode. The wavelength of the monochromated X-ray from Cu Kα radiation is 0.154 nm. The scanning 2θ range was 2–40° with a scanning rate of 5°/min. The basal spacing of the organoclay was estimated from the (001) peak in WAXD patterns.

Two-dimensional wide-angle X-ray scattering (2D-WAXS) experiments were conducted to evaluate crystalline orientation of PA6 matrix using a Rigaku Denki RAD-B diffractometer. The wavelength of the monochromated X-ray from Cu Kα radiation was 0.154 nm and reflection mode was used. The samples were placed with the melt shear flow direction perpendicular to the projection beams.

2.4. Mechanical testing

The central part of tensile specimens with dimensions of $40 \times 6 \times 3.5$ mm was used for impact testing. The impact experiment was carried out on an I200XJU-2.75 Impact Tester according to ISO 180 for Izod test after the specimens notched with 45° at a depth of 1 mm. The fracture propagation direction is perpendicular to the melt shear flow direction. The Izod specimens bend and the pendulum swings by when blends are of high toughness and thus the fracture is incomplete. In this case, only the area of the fractured part was used for calculation and the un-fractured part was deducted. RG T-10 University Testing Machine was used to measure the tensile strength at a speed of 5 mm/min under 20 °C. The values of all the mechanical parameters were calculated as averages over 6–9 specimens for each composition.

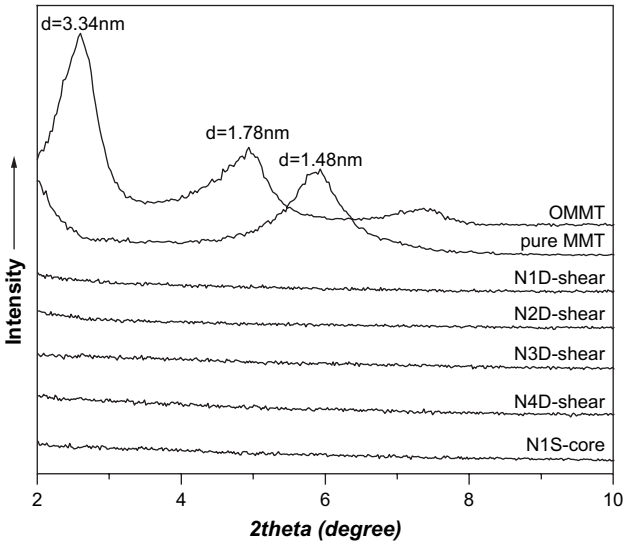

Fig. 2. WAXD photographs of MMT, organoclay and nanocomposites. D and S represent dynamic and static specimens, respectively.

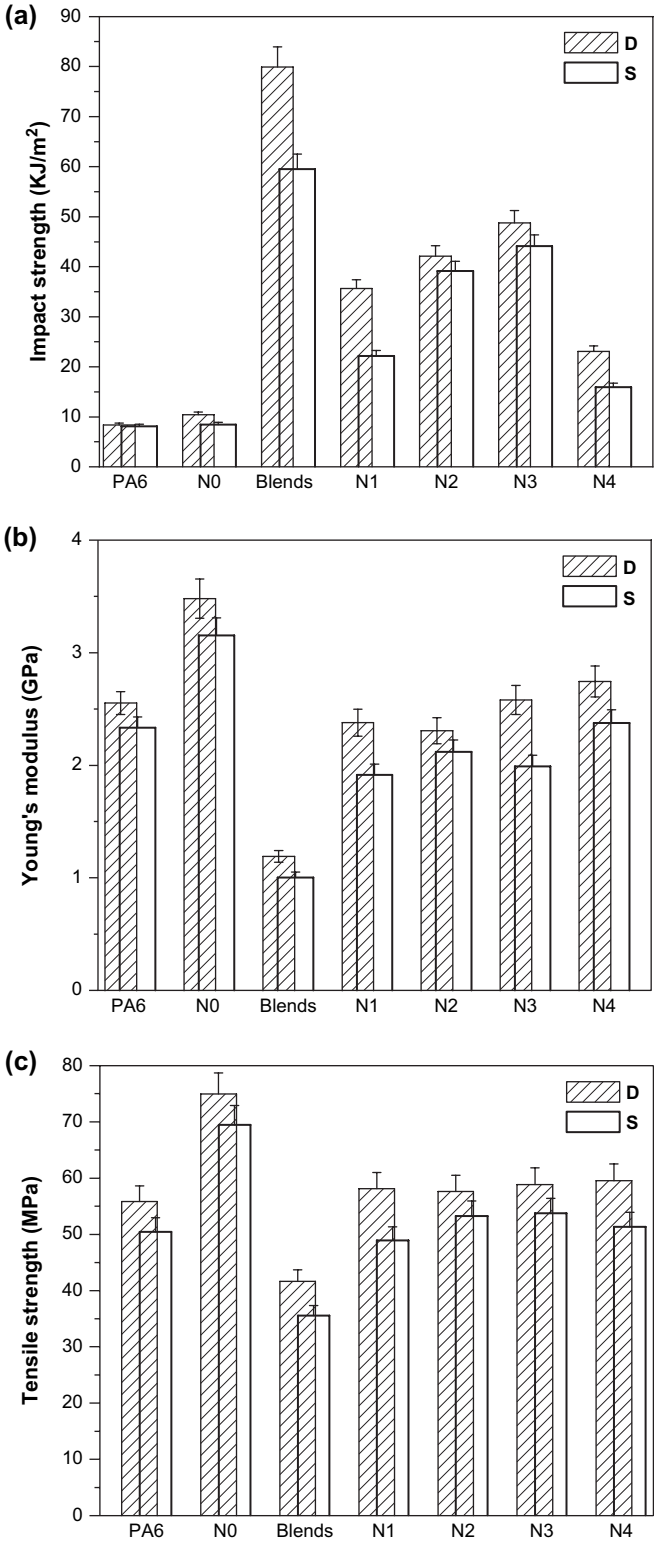

Fig. 3. Graphs of impact strength, Young's modulus and tensile strength of PA6, blends (PA6/EPDM-*g*-MA = 80/20), N0 (PA6/organoclay = 96/4), and N1–N4. D and S represent dynamic and static specimens, respectively.

2.5. Scanning electron microscope (SEM)

The specimens were cryogenically fractured in liquid nitrogen at direction perpendicular to the melt shear flow

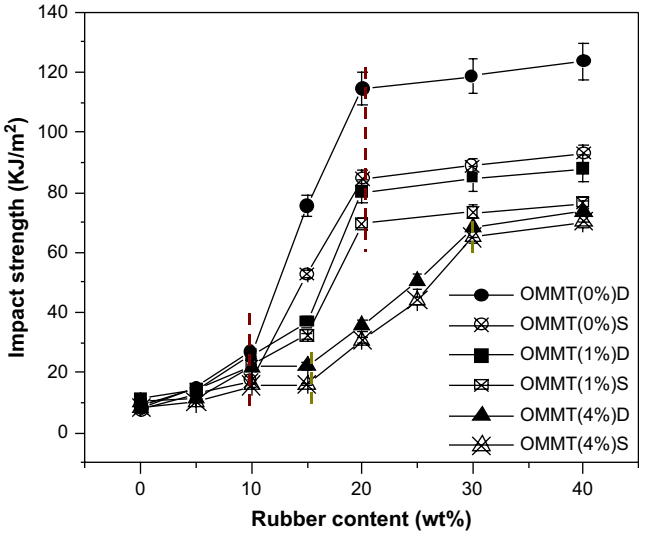

Fig. 4. Rubber content dependence of impact strength in various as-prepared nanocomposites (D and S represent dynamic and static specimens, respectively, and the dash lines indicate the inflexion points of property).

direction (T direction) and parallel to the melt shear flow direction (F direction). Then the fractured surfaces were etched in boiling toluene for 1 h to selectively dissolve the rubber particles. And the phase morphology was observed in a Hitachi X-650 SEM instrument operating at an accelerating voltage of 5 kV after the surface was coated with gold powder.

2.6. Differential scanning calorimetry (DSC)

In a differential scanning calorimeter (Perkin–Elmer DSC Pyris-1), the heating of slice cut from the same place of both static and dynamic specimens were characterized at a scanning rate of 10 °C/min in nitrogen atmosphere. The degree of crystallinity was calculated from heat of fusion using 190 J/g as the heat of fusion of 100% crystalline polyamide 6 [23].

3. Results

3.1. Dispersion of clay in polymer matrix

Fig. 2 shows the WAXD patterns of dynamic specimens of N1–N4, static specimens of N1, pure montmorillonite, and organoclay itself. It is seen in Fig. 2 that the organoclay exhibits a characteristic peak at a 2θ of 2.6° corresponding to *d*-spacing of 3.3 nm. In N1–N4, the characteristic peak of the organoclay disappeared between 2 and 10°. The absence of the characteristic peak of the organoclay in N1–N4 indicates that the clay plates are completely exfoliated in either PA6 or EPDM-*g*-MA, disregarding the blending sequence and processing methods (dynamic or static injection molding). Our result is consistent with the one obtained by Dasari et al. [18]. Since the intercalation and exfoliation of clay in PA6 have been well characterized via WAXD and TEM in the past [11–18], in our work, no further TEM experiment has been carried out for the evidence of clay exfoliation.

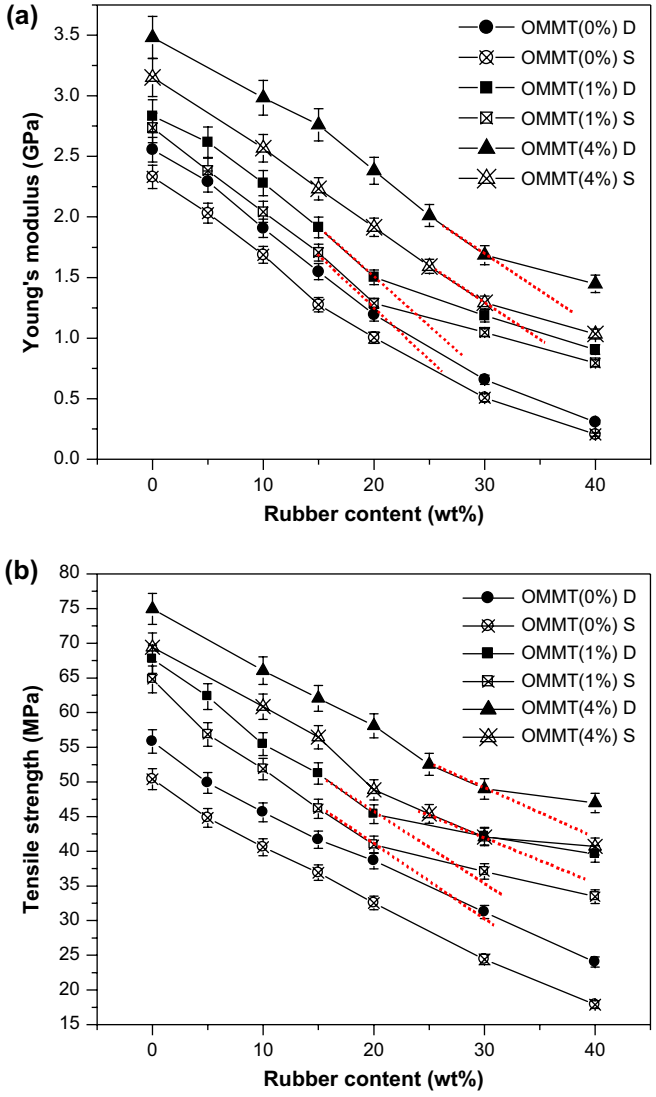

Fig. 5. Plots of Young's modulus and tensile strength against rubber content. D and S represent dynamic and static specimens, respectively.

3.2. Effect of blending sequence and molding methods on the mechanical properties

Fig. 3 shows the impact strength, Young's modulus and tensile strength of pure PA6, binary blends (PA6/EPDM-*g*-MA = 80/20), N0 (PA6/organoclay = 96/4) and ternary composites N1–N4, obtained by using different blending sequence and two molding methods. It should be emphasized, however, that the uncertainties of various mechanical properties shown in Fig. 3 are all less than 5%, ensured a high validity to estimate the impact of processing method on the ultimate properties. One observes a simultaneous increase of impact strength, Young's modulus and tensile strength of PA6 by adding both clay and rubber. The slightly higher values are seen for dynamic samples compared with the static one, and this may

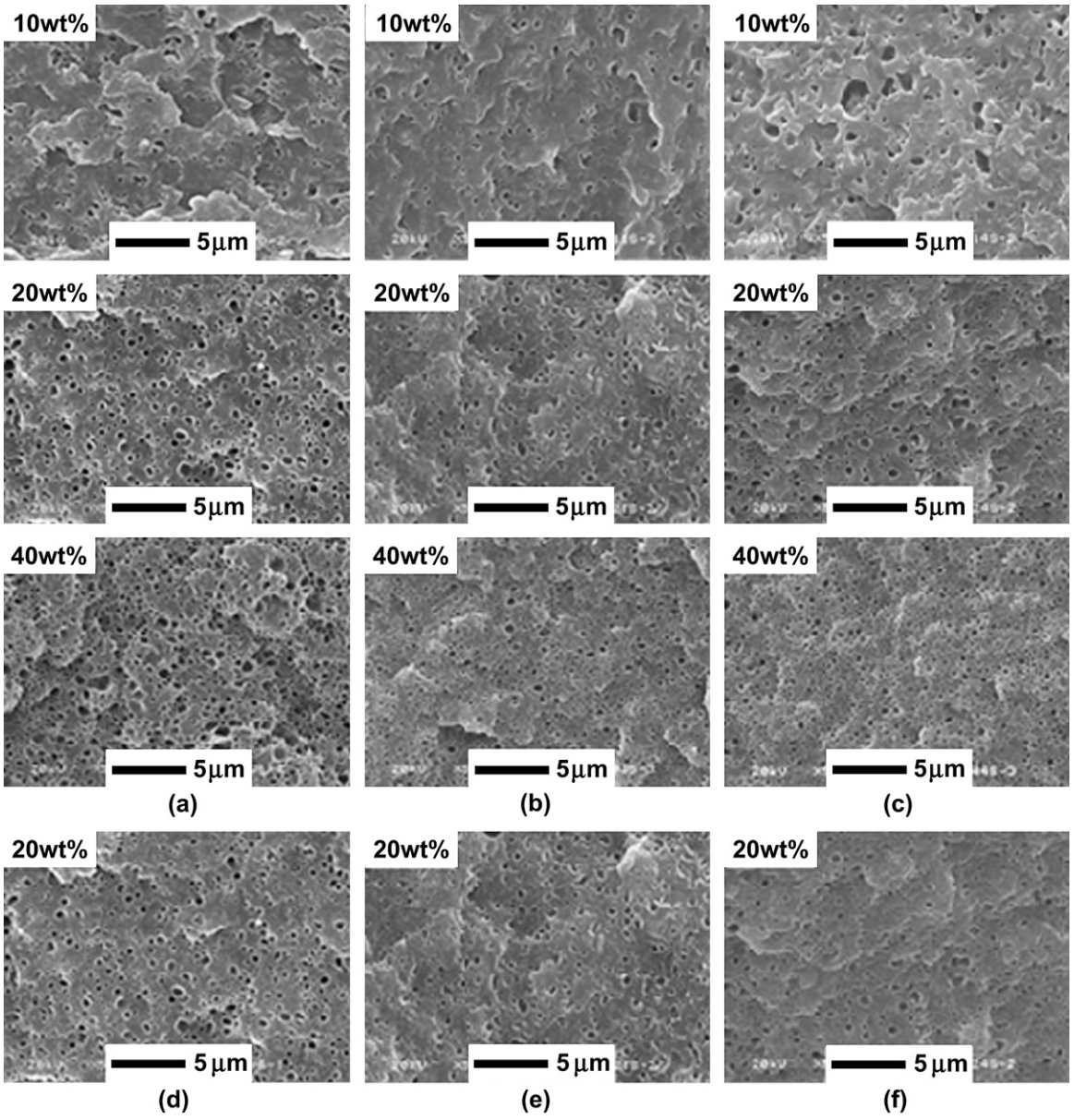

Fig. 6. The SEM photographs got from the core layer of static specimens. (a)–(c) are from F direction without and with 1 wt%, 4 wt% organoclay. (d)–(f) are from T direction without and with 1 wt%, 4 wt% organoclay.

be due to the shear-enhanced interfacial interaction between PA6 and EPDM-*g*-MA or some orientation of the clay layers during dynamic packing injection molding. Although the difference of property between static samples and dynamic samples is not significant, the uncertainty of measured data is small (≤5%) to permit comparing properties between static and dynamic ones. It can be drawn that the mechanical properties of dynamic samples are higher than that of static ones, which is also right in Figs. 4 and 5. Another valuable statement is that there is no significant difference in properties among the blending sequences used. Since one step blending sequence is the simplest way to prepare ternary nanocomposites but still with satisfied mechanical properties and good dispersion of clay, one step blending sequence is used in the following work.

3.3. Effect of clay on the impact strength of ternary nanocomposites

We begin with the impact strength because the toughening of PA6 is always an important issue for PA6 modification. Fig. 4 shows the impact strength of dynamic and static specimens as a function of rubber content. The impact strength of blends without clay is also shown as a reference. It is seen from Fig. 4 that for both the dynamic and static specimens, a sharp brittle–ductile transition occurs at 10–20 wt% of rubber content for specimens without and with 1 wt% organoclay, where a sharp increase of impact strength is observed. However, the impact strength slightly increases with rubber content when rubber content is more than 20 wt%. Comparing to the impact strength of specimens

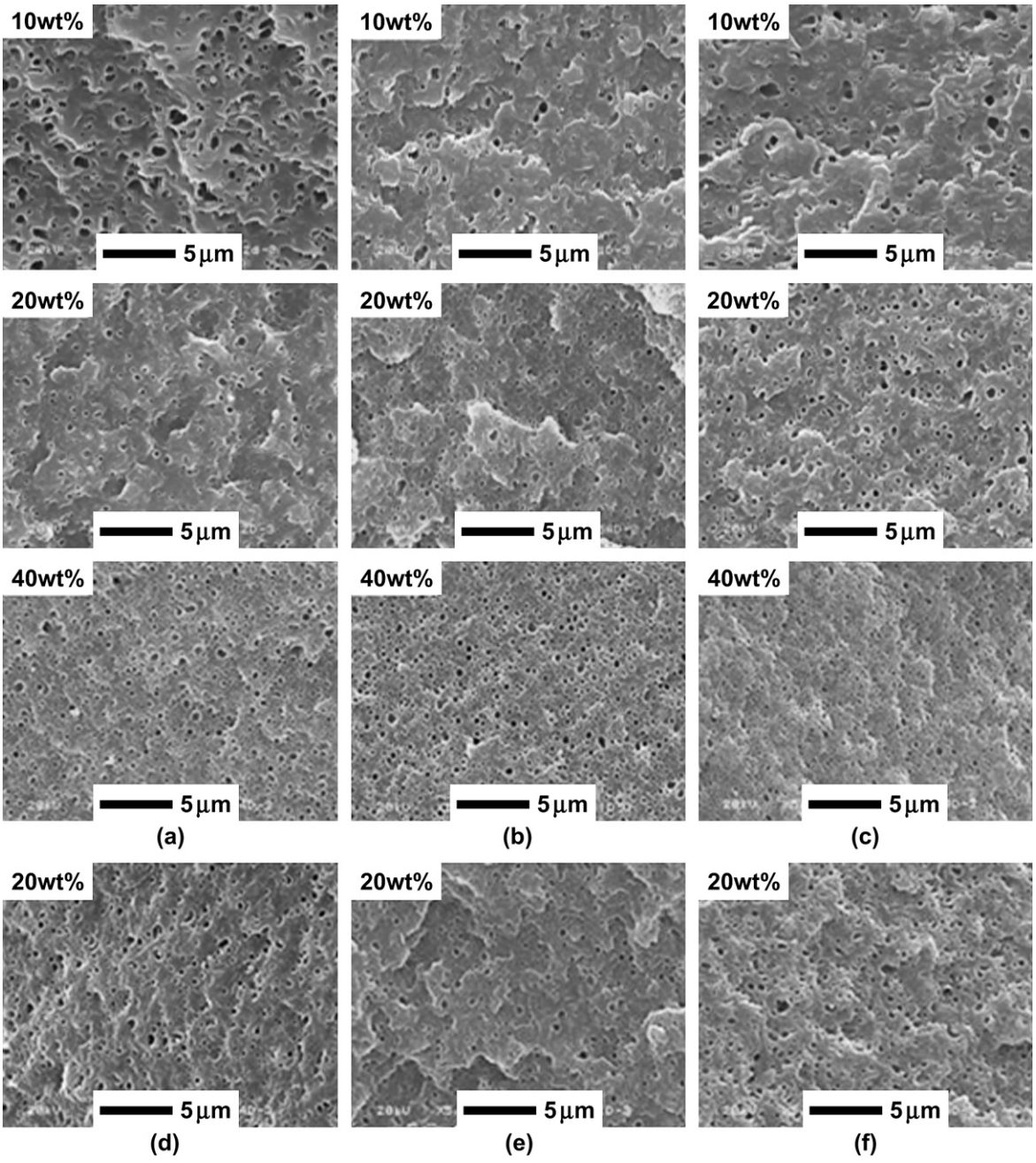

Fig. 7. The SEM photographs got from the core layer of dynamic specimens. (a)–(c) are from F direction without and with 1 wt%, 4 wt% organoclay. (d)–(f) are from T direction without and with 1 wt%, 4 wt% organoclay.

without and with 1 wt% organoclay, the brittle–ductile transition of specimens with 4 wt% organoclay occurs at higher rubber content with much lowered impact strength, and the transition region becomes much broader. In the ductile region, slightly higher values of impact strength are seen for dynamic specimens compared with the static ones, which probably due to the enhanced interaction between PA6 and EPDM-*g*-MA rubber [24] and the possible orientation of clay layers and rubber particles under low shear stress field, but the difference becomes smaller with the increase of organoclay content.

3.4. Effect of clay on the tensile properties of ternary nanocomposites

The tensile properties of specimens without and with organoclay are shown in Fig. 5. The tensile properties increase with increase of organoclay content under the same rubber content. One observes a linear decrease of Young's modulus and tensile strength with increasing of rubber content for binary blends without clay. It is interesting to see that the decrease of tensile properties is not linear with increase of rubber content for the ternary nanocomposites with clay. The

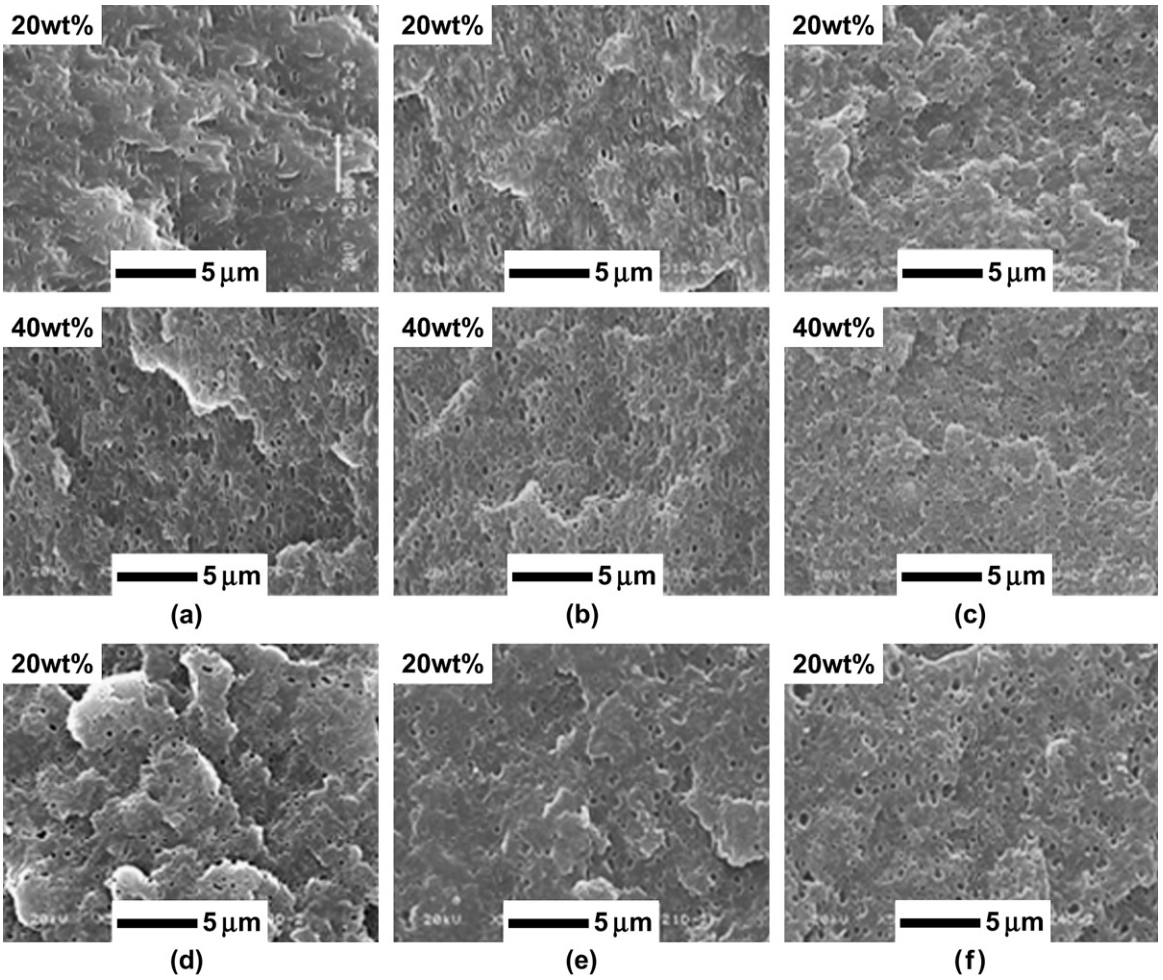

Fig. 8. The SEM photographs got from the shear layer of dynamic specimens. (a)–(c) are from F direction without and with 1 wt%, 4 wt% organoclay. (d)–(f) are from T direction without and with 1 wt%, 4 wt% organoclay.

curves of Young's modulus and tensile strength against rubber content show inflexion points which are located at 20 wt% and 30% rubber content for nanocomposites with 1 wt% and 4 wt% organoclay, respectively. In another words, the decrease of Young's modulus and tensile strength due to the addition of rubber will be more effectively compensated by organoclay when the rubber content was high, resulting a slow downing of the decrease rate of tensile properties.

3.5. Phase morphology

To understand the change of mechanical properties, particularly, the toughening mechanism in these ternary nanocomposites, it is necessary to ascertain dispersion and phase morphology of clay and rubber particles in PA6 matrix. Clay can either locate in the rubber particles or separately disperse in PA6 matrix. Since the strong interaction between PA6 and organoclay, we found in the used processing conditions that the exfoliated clay layers were selectively dispersed in PA6 matrix. This is similar with the result obtained by Khatua [14]. So in our work, we will only investigate the phase morphology of the rubber in these ternary nanocomposites. Usually typical skin-core morphology is obtained in traditional injection molded specimen; for dynamic specimens a shear layer existing between the skin layer and the core layer can be also observed. Because the skin layer is very thin and its effect on mechanical properties could be ignored, we will mainly focus on the shear layer and core layer for the phase morphology investigation. The micrographs of phase morphology of static specimens and dynamic ones in core layer without and with organoclay seen from T (transverse) and F (flow) directions are shown in Figs. 6 and 7, respectively. Combining micrographs from T and F directions it is evident that all the rubber particles are spherical. The rubber particle size of specimens with 1 wt% organoclay is smaller than that of specimens without and with 4 wt% organoclay in the transition region where rubber content is between 10 wt% and 20 wt%. This phenomenon is not similar to those with higher rubber content (more than 20 wt%) and those reported in Refs. [11–14] where the rubber particle size decreased with increase of organoclay content. The presence of organoclay has two competitive effects on phase morphology of nanocomposites. On one hand, organoclay acts as barriers to prevent coalescence of rubber domains and thus causes the decrease

Table 2
Melting point and crystallinity of nanocomposites around the inflexion points

		$X_{PA6}/Y_{EPDM\text{-}g\text{-}MA}/Z_{organoclay}$					
		90/10/1	80/20/1	70/30/1	80/20/4	70/30/4	60/40/4
Melting point (°C)	D-shear	220.26	219.77	219.58	220.27	219.54	219.74
	D-core	220.39	219.94	219.75	220.71	219.58	220.38
	S-core	220.75	220.72	220.10	221.22	220.12	220.46
Crystallinity (%)	D-shear	31.08	28.63	28.3	27.94	26.60	25.86
	D-core	29.77	29.56	26.56	28.93	27.82	27.03
	S-core	26.82	26.87	24.94	28.28	26.65	25.92

of rubber particle size [14]. On the other hand, organoclay will weaken the interface adhesion between PA6 and EPDM-*g*-MA because the shielding effect on the interacting with the MA groups of EPDM-*g*-MA and thus causes the increase of rubber particle size [17]. In the transition region with rubber content of 10–20 wt%, for nanocomposites with 1 wt% organoclay the effect of preventing coalescence of the rubber domains may be dominant while for nanocomposites with 4 wt% organoclay the effect of worsening the interface adhesion between PA6 and EPDM-*g*-MA may be dominant. This could be the reason for the phenomenon specified above. The micrographs of phase morphology of dynamic specimens in shear layer without and with organoclay seen from T and F directions are shown in Fig. 8. Some slightly deformed rubber particles are observed for specimens without and with 1 wt% organoclay. The aspect ratio of stretched rubber particles induced by low shear stress decreases with increase of organoclay content and even no stretched rubber particle is observed in shear layer for specimens contained 4 wt% organoclay.

3.6. DSC results

Since the Young's modulus and tensile strength would be affected by crystalline phase, DSC experiments were carried out to measure crystallinity and melting point of nanocomposites around the inflexion points. The crystallinity is calculated from the equation:

$$\text{Crystallinity} = \frac{\Delta H_f}{\Delta H_f^m \chi_A} \times 100\% \quad (1)$$

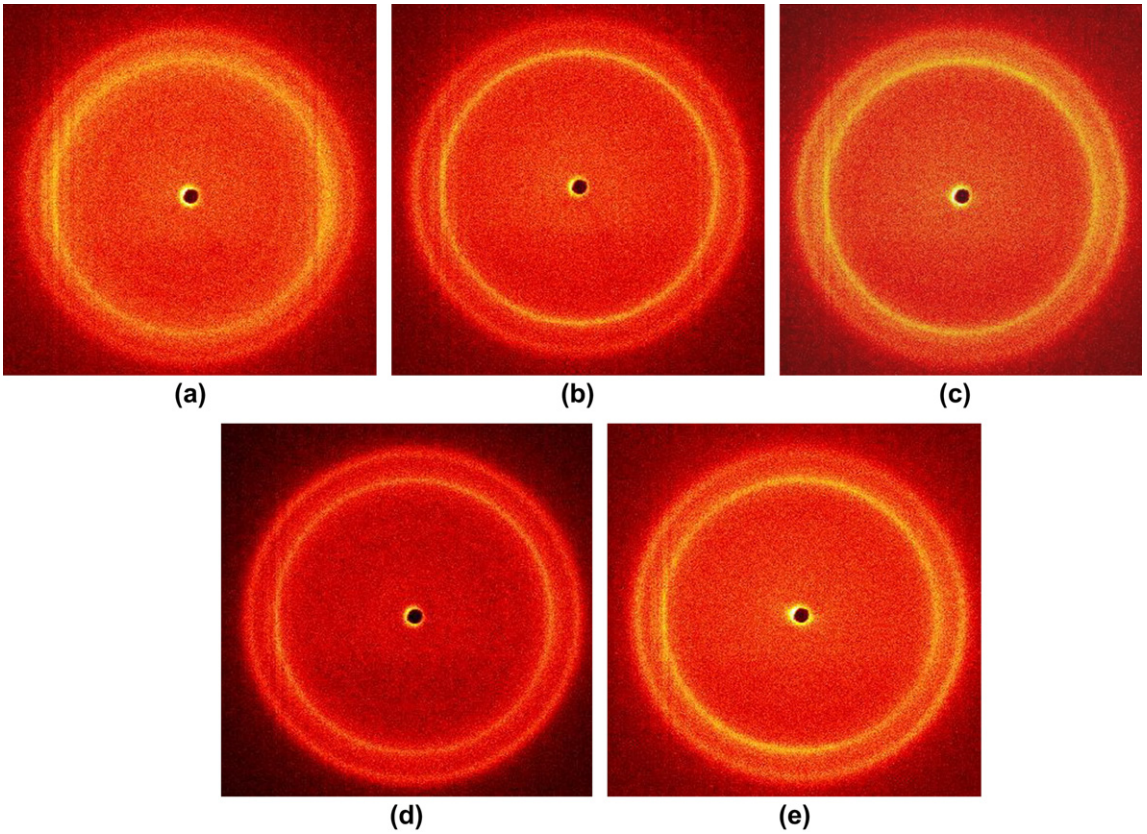

Fig. 9. 2D-WAXS patterns. (a), (b) and (c) are from nanocomposites with 1 wt% organoclay at 10 wt%, 20 wt%, and 40 wt% rubber content, respectively. (d) and (e) are from nanocomposites with 4 wt% organoclay at 20 wt% and 40 wt% rubber content, respectively.

where ΔH_f is the enthalpy of polyamide 6 for the nanocomposites, ΔH_f^m is the enthalpy of polyamide 6 with a crystallinity of 100%, the literature value of 190 J/g is used (α phase). χ_A is the content of polyamide 6 in the nanocomposites. The melting point and crystallinity of dynamic specimens in different layers and static specimens in core layer around the inflexion points are shown in Table 2. Apparently, the melting point around the inflexion points is almost constant which is 220 °C and the crystallinity does not show obvious difference around the inflexion points either.

3.7. 2D-WAXS results

Since the molecular orientation will play a role to determine the mechanical properties, 2D-WAXS experiments were performed to estimate the orientation. Fig. 9 shows the 2D-WAXS patterns of static specimens with rubber content around the inflexion points in core layer parallel to the melt shear flow direction. No distinct oriented structure is evident in each layer as in the cases of PA6/MMT nanocomposites, where a so-called shear amplification mechanism plays a role that a great enhancement of local stress occurs in the small interparticle region of two adjacent layered tactoids with different velocities [25]. The shear amplification effect does not exist in the ternary nanocomposites. So the enhanced mechanical properties are not much related to a change of orientation of PA6 among our specimens. The exfoliated clay could be also oriented along the shear flow direction under the effect of shear; however, its determination is out of the range of 2D-WAXS. Moreover, 2D-SAXS or TEM may be used to check the clay orientation and the ongoing work is to ascertain preciously the dispersion and orientation morphologies of organoclay in ternary nanocomposites using TEM observations.

4. Discussion

4.1. Critical interparticle distance

It is well known that the toughness of rubber filled semicrystalline polymer only depend on the critical interparticle distance τ_c which is the property of the matrix alone. This is quite known as Wu's criterion [26,27]. Considering a log-normal distribution of the particle sizes the interparticle distance τ could be calculated by the equation [23]:

$$\tau = d\left[\left(\pi/6V_f\right)^{1/3}\exp(1.5\ln^2\sigma) - \exp(0.5\ln^2\sigma)\right] \quad (2)$$

where V_f is volume fraction and d is the average diameter of rubber particles. Fig. 10 shows a plot of impact strength versus interparticles distance, which is worked out from the average rubber particle size and particle size polydispersity obtained by image analysis. τ_c could be determined from the inflexion point of the curves which are about 0.29 μm, 0.25 μm, 0.27 μm for blends, nanocomposites with 1 wt% and 4 wt% organoclay, respectively, for both the dynamic and static

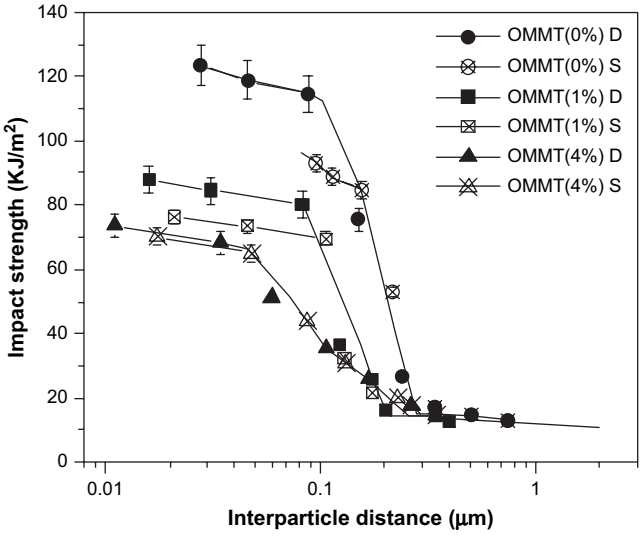

Fig. 10. The impact strength as a function of interparticle distance of PA6/EPDM-*g*-MA blends and nanocomposites with 1 wt% and 4 wt% organoclay. D and S represent dynamic and static specimens, respectively.

samples. It is interesting that within the errors of measurement (about ±10%) in interparticles distance, the critical distance τ_c can be considered as constant with the effect of organoclay, though (1) the brittle–ductile transition regions are not all the same between blends and nanocomposites and (2) the selectively dispersed clay in PA6 makes a changed matrix for the filled rubber particles. Seen from the phase morphology shown in Figs. 6 and 7, in the transition region where rubber content is between 10 wt% and 20 wt%, obviously the rubber particle size of specimens with 1 wt% organoclay is smaller than that of specimens without and with 4 wt% organoclay. Although the rubber particle size is changed due to the addition of organoclay, our result indicates the Wu's criterion holds true for PA6/EPDM-*g*-MA/organoclay ternary nanocomposites. In our system, the toughness of PA6 does not change by adding organoclay (comparing PA6 and N0 in Fig. 3), the matrix property can be considered as constant. Since the τ_c is only the property of the matrix, it is reasonable that Wu's criterion works and the τ_c is kept constant.

4.2. Effect of organoclay on toughening and reinforcing mechanism of ternary nanocomposites

Fig. 11 shows the schematic representations for the role of clay layers on toughness and reinforcement of the ternary nanocomposites. As mentioned in Section 3.3, comparing to the impact strength of specimens without and with 1 wt% organoclay, the transition region becomes much broader for the specimens with 4 wt% organoclay; furthermore, its impact strength is much lower in ductile region. Here we propose a novel mechanism to explain the effect of clay on the toughness of PA6/EPDM-*g*-MA blends, which could be called as the blocking effect of clay layers on the overlap of the "stress volume" between EPDM-*g*-MA particles. According to Wu's toughening theory, the key for the brittle–ductile transition

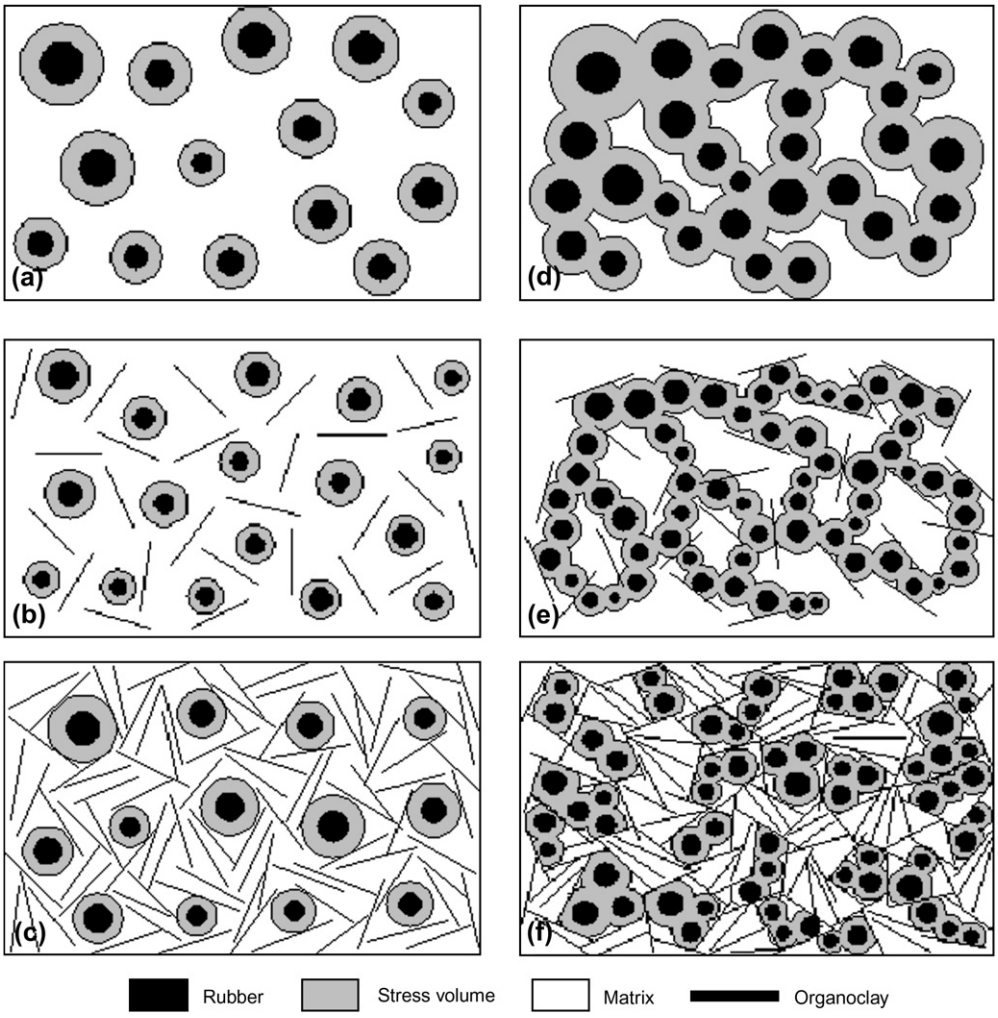

Fig. 11. Schematic representations for the role of clay layers on toughness and reinforcement of ternary nanocomposites. (a), (d) blends; (b), (e) nanocomposites with 1 wt% organoclay; (c), (f) nanocomposites with 4 wt% organoclay. For (a), (b) and (c) $\tau > \tau_c$, and (d), (e) and (f) $\tau < \tau_c$.

is the overlap of stress volume between EPDM-*g*-MA particles as the interparticle distance below a critical value. It is expected that presence of clay layers in PA6 matrix will block the overlap of the "stress volume". When the content of clay is small (such as in the case of specimens with 1 wt% clay), the blocking effect is weak, and the toughness and the transition do not change much comparing that of the blends, the schematic representation could be demonstrated in (b) and (e) of Fig. 11. However, when the content of clay is high (such as in the case of specimens with 4 wt% clay), the formation of clay network is most likely [28–31]. In this case, it is expected that the clay network will block the overlap of the stress volume between EPDM-*g*-MA particles in a large extent, thus a broadening of transition and decreased toughness are observed. The schematic representations could be demonstrated in (c) and (f) of Fig. 11.

Now let us discuss the nonlinear decrease of tensile properties with increase of rubber content for the ternary nanocomposites with clay. There are four possible explanations to this phenomenon. The first one is that the dispersion state of organoclay could be different among these samples since the exfoliated systems give better mechanical properties than intercalated ones. But evident from the WAXD patterns in Fig. 2, one knows that the organoclays for all nanocomposites investigated are exfoliated disregarding the rubber content. So the change of dispersion state of organoclay is not the reason for this phenomenon. The second one is that the crystallinity could be changed around the inflexion points which could also result in a change of tensile properties. From Table 2 it is clear that the crystallinity does not change too much around the inflexion points. So the change of crystallinity has nothing to do with this phenomenon either. The third one is that the orientation state of PA6 macromolecules could be changed around the inflexion points. But the 2D-WAXS patterns in Fig. 9 do not show any evidence of oriented structure around the inflexion points. Therefore, the effect of orientation of PA6 macromolecules could also be excluded. With an eye to the inflexion points occur just at the end of the brittle–ductile transition region, so the last possibility might be that when the rubber content is higher than the inflexion points where the interparticles' distance τ is smaller than the critical interparticle distance τ_c, in this case the stress volume around the rubber

particles percolates throughout the specimens, and the load could be transferred from one clay layer to another by the percolated stress volume. When small-strain properties such as modulus of elasticity are measured, organoclay has better reinforcement effect, as shown in Fig. 11(e) and (f). While as $\tau > \tau_c$, the stress volume around rubber particles has no chance to be interacted, thus the role as stress transfer between clay layers is not possible. The schematic representations are demonstrated in (b) and (c) of Fig. 11.

5. Conclusion

In summary, we find that blending sequence has not much influence on the mechanical properties and one step blending sequence already had satisfied balanced mechanical properties for PA6/EPDM-*g*-MA/organoclay ternary nanocomposites. The dynamic packing injection could lead to a better mechanical properties compared to traditional injection molding, due to the enhanced interaction between PA6 and EPDM-*g*-MA rubber and the possible orientation of clay layer and rubber particles. According to SEM micrographs, it is clear that organoclay has two competitive effects. One is the effect of worsening interface adhesion; another is effect of preventing coalescence of rubber domains. Concerning impact strength of ternary nanocomposites, blocking effect on overlap of the stress volume and the effect of worsening interface adhesion would reduce the impact strength of these materials. The decrease of Young's modulus and tensile strength due to the addition of rubber will be more effectively compensated by compounding with organoclay at higher rubber content, resulting a slow down of the decrease rate of tensile properties.

Acknowledgements

We would like to express our sincere thanks to the National Natural Science Foundation of China for Financial Support (20404008, 50533050, 50373030 and 20490220). This work is subsidized by the Special Funds for Major State Basic Research Projects of China (2003CB615600).

References

[1] Tjong SC, Meng YZ, Hay AS. Chem Mater 2002;14:44.
[2] Krikorian V, Kurian M, Galvin ME, Nowak AP, Deming TJ, Pochan DJ. J Polym Sci Part B 2002;40:2579.
[3] Tang Y, Hi Y, Song L, Zong RW, Gui Z, Chen ZY, et al. Polym Degrad Stab 2003;82:127.
[4] Li J, Zhou C, Wang G, Zhao D. J Appl Polym Sci 2003;89:3609.
[5] Lee JY, Lee HK. Mater Chem Phys 2004;85:410.
[6] Ray SS, Okamoto M. Prog Polym Sci 2003;28:1539.
[7] Hussain F, Hojjati M, Okamoto M, Gorga RE. J Comp Mater 2006;40:1511.
[8] Usuki A, Hasegawa N, Kato M, Kobayashi S. Adv Polym Sci 2005;179:135.
[9] Maniar AA. Polym Plast Technol Eng 2004;43:427.
[10] Pinnavaia TJ, Brall GW, editors. Polymer-clay nanocomposites. New York: John Wiley & Sons; 2000.
[11] Gelfer MY, Song HH, Liu L, Hsiao BS, Chu B, Rafailovich M, et al. J Polym Sci Part B 2003;41:44.
[12] Voulgaris D, Petridis D. Polymer 2002;43:2213.
[13] Wang Y, Zhang Q, Fu Q. Macromol Rapid Commun 2003;24:231.
[14] Khatua BB, Lee DJ, Kim HY, Kim JK. Macromolecules 2004;37:2454.
[15] Chow WS, Ishiaku US, Mohd Ishak ZA, Karger-Kocsis J, Apostolov AA. J Appl Polym Sci 2004;91:175.
[16] Chiu FC, Lai SM, Chen YL, Lee TH. Polymer 2005;46:11600.
[17] González I, Eguiazábal JI, Nazábal J. J Polym Sci Part B 2005;43:3611.
[18] Dasari A, Yu ZZ, Mai YW. Polymer 2005;46:5986.
[19] Guan Q, Shen KZ, Li J, Zhu J. J Appl Polym Sci 1995;55:1797.
[20] Wang Y, Fu Q, Li QJ, Zhang G, Shen KZ, Wang YZ. J Polym Sci Part B 2002;40:2094.
[21] Na B, Zhang Q, Fu Q, Zhang G, Shen KZ. Polymer 2002;43:7367.
[22] Zhang Q, Wang Y, Fu Q. J Polym Sci Part B 2003;41:1.
[23] Liu ZH, Zhang XD, Zhu XG, Qi ZN, Wang FS. Polymer 1997;38:5269.
[24] Wang C, Su JX, Li J, Yang H, Zhang Q, Du RN, et al. Polymer 2006;47:3197.
[25] Yalcin B, Valladares D, Cakmak M. Polymer 2003;44:6913.
[26] Wu S. J Appl Polym Sci 1988;35:549.
[27] Margolina A, Wu S. Polymer 1988;29:2170.
[28] Galgali G, Ramesh C, Lele A. Macromolecules 2001;34:852.
[29] Solomon MJ, Almusallam A, Seefeldt K, Somwangthanaroj A, Varadan P. Macromolecules 2001;34:1864.
[30] Schmidt G, Nakatani AI, Han CC. Rheol Acta 2002;41:45.
[31] Lin-Gibson S, Kim H, Schmidt G, Han CC, Hobbie EK. J Colloid Interface Sci 2004;274:515.